Maritime Economics & Logistics (2023) 25:452–478
https://doi.org/10.1057/s41278-023-00263-z

ORIGINAL ARTICLE

Understanding the implications of port-related workforce shortages on global maritime performance through the study of a carrier alliance

Wenjie Li[1] · **Elise Miller-Hooks**[1]

Accepted: 6 June 2023 / Published online: 26 June 2023

Abstract
Maintaining a full workforce is critical to the operational efficiency of ports, which are key to the functioning of global maritime transportation systems, as well as to the larger logistics systems and the industries they support. A shortage of skilled workers, or extended, large-scale, absenteeism at one or more ports can affect cargohandling operations, competitiveness, and even the efficiency of international trade. Through numerical experiments, we study (i) whether the effects of low-level workforce shortages can be 'absorbed' without loss of efficiency; (ii) the level at which shortages in a region can impact another region, or the performance of the wider maritime system. To test this, we investigate the ports used by the M2 shipping alliance of Maersk Line and Mediterranean Shipping Company. The analysis is supported by advanced mathematical modeling and algorithmic procedures. Findings include that low- and even mid-level network-wide worker shortages can be absorbed, but at a greater cost to shippers. Moreover, when a worker shortage arises in some regions of the world, the impacts in other regions can be very significant.

Keywords Labor shortage · Workforce absenteeism · Unfulfilled job vacancies · Global maritime system · Port networks · Port resilience

1 Introduction

Modern industries and distributors rely on logistics providers to deliver services and thereby minimize their need to invest in and maintain inventory. In a worldwide economy, manufacturing conducted in any region will be supported by materials from disparate locations and will provide end products to local markets across the globe. The needs of these industries include not only demand for shipping final

✉ Elise Miller-Hooks
miller@gmu.edu

[1] Department of Civil, Environmental and Infrastructure Engineering, George Mason University, Fairfax, VA 22030, USA

products, but also raw materials and middle products. Global logistics systems, thus, maintain the needed flow of raw and manufactured materials to the market on time. As such, it is paramount that transportation and distribution systems that support these industries or distributors provide reliable services and infrastructure that can support their demand.

With this reliance on logistics systems, global and local economies depend on a well-functioning maritime system. Important to the success of the system is the capability of ports to receive and transship materials and products to their final destinations with minimal delays. Maintaining capacity to receive, transship, and ship out cargo, referred to as port throughput capacity, is a critical aspect of maintaining efficient global logistics services. If a port accepts to serve cargo and cannot effectively process it, the larger logistic system loses efficiency. This loss in efficiency reverberates through the manufacturing system leading to increased costs for industry.

Skilled longshore workers, truck drivers, crane and gantry lift operators, warehouse workers and managers, and numerous other types of skilled staff are key to the functioning of ports, and ports are key to the functioning of global maritime transportation systems and the supply chains they support. Unfulfilled job vacancies or extended absenteeism, as occurred during the early stages of the COVID-19 pandemic at certain ports, affect cargohandling operations and can impair a port's competitiveness (Notteboom et al. 2022). In 2021, 77% of the world's largest ports faced backlogs of laden containers due to port-related worker shortages. These containers were stored in yards or on vessels anchored outside the port's channels, waiting at times for long periods for an opening to berth (Kay 2021). In 2020–2022, shortages in professional truck drivers and yard equipment operators across the globe led not only to backups at the ports, but caused further shortages of equipment, such as chassis, throughout the logistics systems (as noted by Cullinane and Haralambides (2021), Kay (2021), Merk et al. (2022), and Mongelluzzo (2022a)).

As further evidence of the impact of worker shortages, consider the ports of Los Angeles and Long Beach (LA-LB) in California. Due to very high positive cases of COVID-19 among skilled longshore workers who drive container-movement equipment, the turnaround time for a container nearly doubled in 2022, as compared with average times from 2017 to 2019 (Mongelluzzo 2022b). Moreover, the average truck turn time increased by 18% in the 6 months between July of 2021 and January of 2022, and chassis dwell times increased three-fold from the pre-pandemic average of four days (Mongelluzzo 2022a).

This paper investigates the global impacts of regional or worldwide port-related worker vacancies or events of sustained absenteeism (i.e., worker shortages) on maritime system performance related to global container flows. Such a system consists of container terminals at ports, maritime routes, and containerships of various types and sizes. Through numerical experimentation on a high-fidelity representation of the global port network, we study whether the effects of low-level worker shortages can be absorbed, in terms of meeting shipping demand, and at what level shortages in a region can impact performance of the wider, global maritime system. The paper further considers if the effects of a labor shortage in one region can extend into other regions. To this end, a set of metrics are assessed under 91 labor level-related

scenarios (30 network-wide, 60 region-wide and an idealized base case). Annual transported cargo in number of TEUs by origin–destination (O-D) pair, inbound and outbound cargo flows in twenty-foot equivalent units (TEUs) at ports, and cargo flows in TEUs along operational routes are estimated under these 91 scenarios with the goal of quantifying the effects of considered labor shortage scenario.

The investigation employs a mathematical formulation, a capacity-constrained, mixed-integer linear program (MILP), in which vessel and container flows through the global port network are replicated assuming that carriers seek to minimize their transport costs. Linear, square, and exponential workforce level-dependent cargo-handling times at the ports, and capacities that limit the number of containers per year that a port can process model various levels and impacts of worker shortage events. Exact solution of the mathematical model is obtained through a path-based Benders decomposition methodology. The model and solution method are presented in Appendix A. Findings are presented from a case study using network data from one of the world's largest container shipping alliances, 2 M, for several potential port-related worker shortage scenarios with regional and global impact. The network representation involves 77 nodes representing ports, and includes 32 routes, 338 links, and 4,110 legs as described in Sect. 4. Insights into the impacts of port-related worker shortages on global maritime system performance are presented in Sect. 5. Conclusions and discussion are given in Sect. 6. The next section describes related literature and establishes the gap that this paper fills.

2 Related Works

Miller-Hooks (2023) proposed the concept of human infrastructure in the context of constructs for framing general infrastructure resilience. Her work recognizes the impacts of staff shortages on the capacity of the built environment to provide services, and the effectiveness with which such services can be offered. This idea is employed here by considering the role of labor in the capacity of the maritime system. Consistent with this concept, the effects of labor shortages have been studied in the context of supply chains (e.g., Lewis et al. 2006; Nagurney 2021a, b; Nagurney and Ermagun 2022; Ergun et al. 2023). Disruptions due to labor shortages on supply chain system resilience were considered by Ergun et al. (2023). They found that labor shortages associated generally with transport logistics can lead to service interruptions and influence supply chain resilience. Nagurney (2021a, b) incorporated labor as a constrained resource for supply chains and studied its impact on supply chain performance using an optimization modeling approach. Constrained product flows resulting from reduced labor availability was shown to affect the profits of participating firms in the COVID-19 pandemic. Impacts of labor availability on supply chain networks were further studied in (Nagurney and Ermagun 2022). This work investigated the impacts of disruptions resulting from reduced productivity on the efficiency and resilience of supply chain networks. In all these works, a simplified representation of the transportation network, including only inland networks, with no mention of maritime involvement, was employed. Lewis et al. (2006) estimated the costs of inventory holding and delay penalties for a firm that operates a supply chain using a seaport that incurs an unexpected

closure. They mention labor shortage as a possible cause for the closure. While also simplistic in its representation of the transportation system, this work does consider the importance of labor to a port and supply chain operations. More recently, the impact on global container shipping and port operational resilience during workforce shortages in the COVID-19 pandemic was discussed in Notteboom et al. (2021).

Worker shortage impacts have been considered in other arenas, such as health care systems (e.g., Hu et al. 2016; Shahverdi et al. 2020) and construction management (e.g., Kim et al. 2020). Examples in the context of health care systems include works by Hu et al. (2016) and Shahverdi et al. (2020) who studied workforce shortages in hospitals. Hu et al. (2016) developed an infinite-horizon model to plan health workforce for a large health care system. Shortages in nurses were considered as a key factor in planning. Shahverdi et al. (2020) simulated operations of patient flows for multiple hospitals and investigated the impact of hazard events on the availability of personnel resources, including nurses, doctors, and skilled technicians. The authors investigated the effects of reduced labor availability on emergency patient service capacity. Kim et al. (2020) used a simulation-based system-dynamics model to examine the effects of skilled labor shortages on the construction industry. Their model aimed to understand the dynamic relationships between industry reputation, lack of worker training, and low initial wages causing worker shortages and the impacts of the shortages on labor wages, cost overruns, and schedules associated with a construction project.

Some works have also considered other causes of reduced port capacity utilization that can lead to increased cargohandling times in port and affect the efficiency of international trade. Port disruption impacts on the performance of the global maritime network from hazard events, such as caused by earthquakes and storms, can impact port operations as studied in (Asadabadi and Miller-Hooks 2018; Achurra-Gonzalez et al. 2019; Li et al. 2022). The impacts of these hazards were modeled in these earlier works for highly aggregated global network representations (with only six nodes, each representing as much as a continent). These works considered total shipping costs, unmet demand, port system or component resilience, as well as mitigation strategies. While worker shortage may not be due to physical damage, these events will lead to increased cargohandling times in port and reduced port capacities; thus, they can similarly affect port performance.

While there are several works that study worker shortage impacts, it appears that no work in the archived literature has investigated the impacts of port-related worker shortages on the performance of the maritime system. This paper aims to fill this gap through the study of outcomes of systematically designed numerical experiments on a high-fidelity representation of the global port network under varying scenarios associated with worker availability.

3 Methodology Overview

To investigate the effects of port-related worker shortages on the functioning of the global maritime transportation system, a cargo flow optimization model is introduced and solved. The model determines an optimal flow of containerships

through ports and along maritime routes given port and route capacities, sailing times, cargohandling times in port, and route operational costs for specified worker levels at chosen ports. Optimality is defined in terms of minimizing total operational costs. In addition to changes in total transportation costs that can result from worker shortages, changes in satisfied demand and port throughput can be affected. A comparison of results of runs to results with base labor levels in terms of these and other metrics provides insights into port-related worker shortages. The mathematical formulation of the cargo flow optimization model and an exact methodology based on concepts of Benders decomposition for its solution are presented in Appendix A. The formulation is a mixed-integer program, a capacitated network flow model, that seeks optimal containerized cargo flows through the maritime system given linear, square, or exponential workforce level-dependent cargohandling times at the ports.

4 Experimental Design

To determine the impact of a port-related worker shortage on the performance of the maritime network, the proposed cargo flow optimization model $P(r_p)$ in Appendix A was applied on a representation of the global maritime network. The Benders decomposition method described in Fig. 7 was implemented in Python 3.9 using off-the-shelf software Gurobi 9.5.1. Numerical experiments were run on a personal computer with Intel Core i9-10850 K CPU 3.60 GHz and 32.00 GB of RAM. Details of the experimental design and results are given in the remainder of this section.

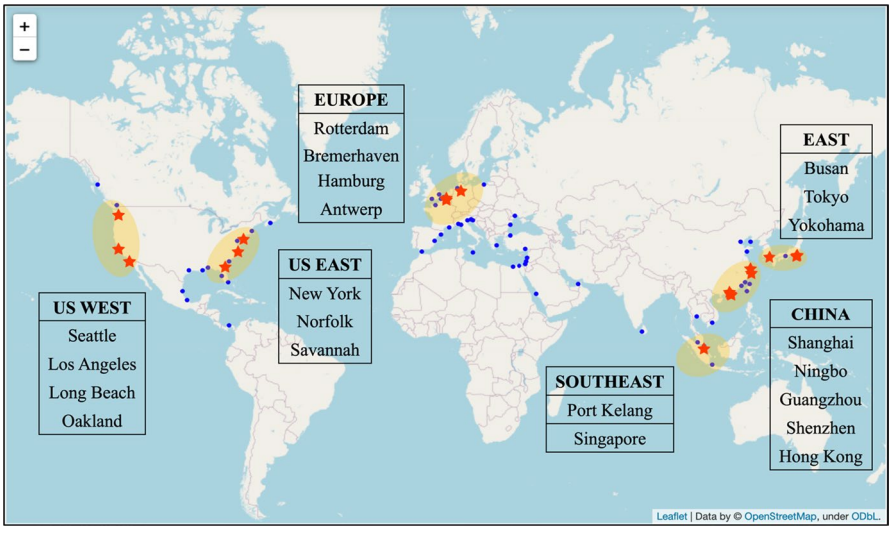

Fig. 1 Ports (dots), regions (shaded ovals), ports chosen for inclusion in a region (stars)

4.1 Network Setting

The model was applied on a network representation of the global maritime system as operated by the 2 M Alliance (Maersk and Mediterranean Shipping Company), which holds a global market share in container-based ocean transportation of approximately 30% (Statista 2022). The network representation consists of 77 ports, 32 routes, 338 links, 4110 legs, with 2 classes of container ships with capacities of 8000 and 12,000 TEUs. Two types of containerships are set with different speeds and fuel consumption rates. The larger vessels consume more fuel per unit of time. The settings were obtained from (Li et al. 2021) and are provided in Appendices B (containerized cargo demand), C (ports), and D (routes) for completeness. Port throughput capacity limits the total inbound and outbound number of TEUs that can be handled at the port annually.

Also important is the capacity of the transportation links and the availability of assets to meet the requirements of the ports to receive and distribute goods. Route capacity, in practice, includes required vessel and ground transportation capacities, as well as storage capacity needed to manage the flow of materials and products to their destinations. Herein, route capacity is defined by the limit on the annual available number of transits by vessels along each route, i.e., by vessel capacities and annual number of vessel transits. Network inputs, including annual port throughput capacities and route capacities, were scaled for consistency with 30% of global container demand assumption.

To investigate the impacts of regional port-related worker shortage scenarios, six regions were designated, each representing a subgroup of major ports from the 77 modeled ports. These include the West Coast and East Coast of the United States (US WEST and US EAST), the Western Europe (EUROPE), the Malacca Strait (SOUTHEAST), the Coast of China (CHINA), and East Asia (EAST). Only the top five ports with annual throughput capacity of at least 2,000,000 TEUs per year are included in each region. 21 of the 77 ports are, thus, included in one of these six regions. These 21 ports account for approximately 65% of total port throughput of the larger network. These regions and the relationship of the 77 ports included in the network to these regions are illustrated in Fig. 1.

4.2 Design of Experiments

Numerical experiments were designed to include 91 runs, including a base run (Run 0) in which all job vacancies are filled and absenteeism is at a typical level. The remaining 90 runs align with various settings of changing workforce level, ranging from 0 to 0.9, taken in 0.1-increments for each of the three port workforce level-dependent performance functions (18, 18′ and 18″ in Appendix A). A workforce level setting of 0 implies a worst case in which the port is closed. The first 30 runs were conducted to test worker shortages occurring at all ports in the network. Each set of 10 runs (of the 30) corresponds to the range of workforce levels and to one of the three workforce level-dependent performance functions (18, 18′ and 18″). An additional 60 runs were

conducted to assess the impact of a worker shortage at the ports, in any one of the six regions ($e \in E$, for E the set of all regions). For each region, a batch of 10 runs was completed for varying workforce levels. Workforce level-dependent performance function (18′) was used in all 60 runs.

4.3 Measures Used in Result Analysis

Results of the runs were analyzed by five measures: (1) satisfied demand, SD; (2) satisfied demand rate, SDR; (3) individual ($T_p, p \in P$); regional (REG_T_e, $e \in E$), and network-wide (NET_T) port throughput; (4) port throughput comparison to baseline, $F_p, p \in P$; and (5) regional vulnerability.

The first term, satisfied demand, is measured in number of delivered TEUs and is computed by Eq. (1), where D_{od} is the containerized cargo shipment demand given as parameters of the model, and $\overline{u_{\text{od}}}$ is the optimal value of decision variable u_{od}.

$$\text{SD} = \sum_{\text{od} \in \text{OD}} \left(D_{\text{od}} - \overline{u_{\text{od}}}\right). \tag{1}$$

In Eq. (2), the satisfied demand rate is computed as a ratio of number of delivered TEUs for a given run divided by number of delivered TEUs in the base run (Run 0), where $u_{\text{od}}{}^*$ gives the number of undelivered TEUs under Run 0.

$$\text{SDR} = \sum_{\text{od} \in \text{OD}} \left(D_{\text{od}} - \overline{u_{\text{od}}}\right) / \sum_{\text{od} \in \text{OD}} \left(D_{\text{od}} - u^*_{\text{od}}\right). \tag{2}$$

Port throughput is computed in Eq. (3). It is taken as the sum of the port's inbound and outbound containerized cargo flows (in TEUs), $\overline{y^v_\phi(i,p)}$ and $\overline{y^v_\phi(p,j)}$, respectively. $P(e)$ denotes the ports in region e, $e \in E$. Regional, REG_T_e, and network-wide,NET_T, port throughputs are computed from the sum of their constituent port throughputs as in Eqs. (4) and (5).

$$T_{\text{p}} = \sum_{v \in V} \sum_{\phi \in \Phi} \sum_{l^v_\phi(i,p), l^v_\phi(p,j) \in L(\Phi)} \left(\overline{y^v_\phi(i,p)} + \overline{y^v_\phi(p,j)}\right), \forall p \in P \tag{3}$$

$$\text{REG\_}T_e = \sum_{p \in P(e)} T_p, \forall e \in E \tag{4}$$

$$\text{NET\_}T = \sum_{p \in P} T_p \tag{5}$$

Port throughput comparison to baseline of an individual port is set to the ratio of port throughputs under a given worker level scenario to port throughputs obtained in the base run (Run 0) in Eq. (6), where T^*_p, $p \in P$ is the port throughput from Run 0.

$$F_p = T_p / T^*_p, \forall p \in P \tag{6}$$

Regional port throughput for each region $e \in E$, REG_T_e, is computed through Eq. (4). To evaluate the impact of a change in workforce level, incurred in a particular region, on regional port throughput for each region, a correlation matrix is calculated. Each element of the matrix provides a number between -1 and 1, indicating the intensity of impact of a reduction in workforce level in one region on another. 1 indicates that the reduction rate in throughput at the ports in the affected region will be identical to the reduction rate in the second region and a -1 indicates that this reduction will have the opposite effect on the throughput of ports in the second region.

5 Results and Findings

5.1 Impacts of Network-wide Port-related Worker Shortage

Results of the first 31 runs associated with network-level performance under network-wide worker shortage scenarios are provided in Figs. 2 and 3. As shown in these figures, performance is significantly impacted by the workforce level-dependent performance function that is presumed. Using an exponential workforce level-dependent performance function as suggested in (Schofer et al. 2022), the results indicate that even small reductions in worker levels can significantly impact overall system performance.

With a linear performance function, greater reductions could be absorbed with less system-wide impact. Figure 3 further reveals that some ports may benefit from initial (smaller) system-wide reductions. Through deeper analysis of the results, the port throughput comparison to baseline at Port of Le Havre in France increases to 1.8 when the port workforce level is 0.9 under a linear workforce level-dependent

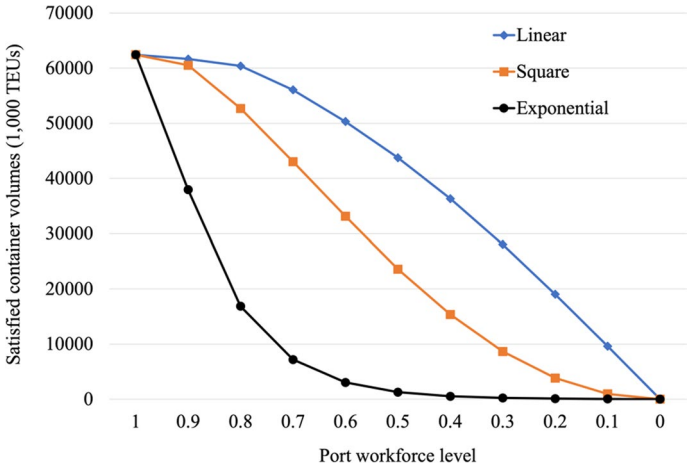

Fig. 2 Number delivered TEUs under network-wide worker shortage scenarios and varying workforce level-dependent performance functions

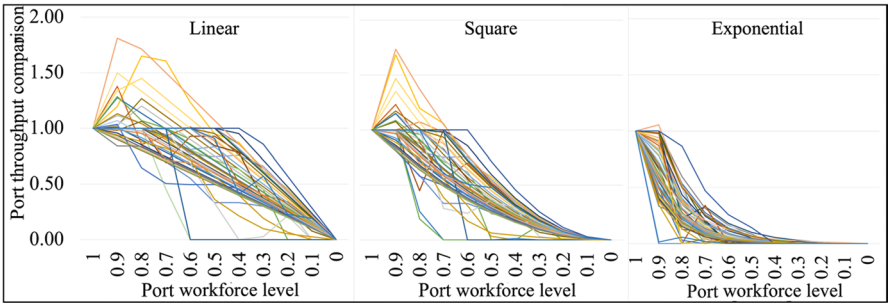

Fig. 3 Port throughput comparison to baseline of 77 ports with network-wide changing workforce levels under three workforce level-dependent performance functions

performance function, while the port throughput comparison to baseline at the Ports of Zeebrugge in Belgium and Tanjung Pelepas in Malaysia, for example, quickly decreases to zero under an exponential workforce level-dependent performance function even with a network-wide port workforce level of 0.9. The majority of shipments handled at these ports concern transshipment. With reduced capacities and longer handling times, these ports lose their attractiveness for such services, which may become more attractive at alternative ports.

5.2 Impacts of a Regional Port-related Worker Shortage

5.2.1 Impacts on the maritime network

In Fig. 4, the closure of ports in the CHINA and SOUTHEAST regions has the most and least reductions in satisfied demand, respectively. For low levels of worker shortage in any of the regions, there is no reduction in satisfied demand.

Figure 5 plots curves of satisfied demand rates of 1.00, 0.90, 0.80, and 0.50. Workforce level and satisfied demand rates are set to 1 in Run 0. The 1.00 curve indicates that the maritime system fully absorbs the impacts of a worker shortage at the ports in the relevant region. The lowest workforce levels for the six regions with no reduction in satisfied demand range from 0.60 (region SOUTHEAST) to 0.90 (regions US WEST, EAST, and US EAST). The 0.50 curve indicates that half the demand could not be transported by the maritime system. This occurs when workforce levels in the CHINA region sink below 0.2. Note that the 50% reduction in satisfied demand for a 80% reduction in workforce level at affected ports occurs with a presumed square workforce level-dependent performance function. That is, the network-wide reduction in satisfied demand is less than the effect on the port-related cargohandling times and throughput capacities in the region, perhaps because only a subset of ports incur a worker shortage. Ports with worker shortages will have reduced capacities to service vessel traffic, while those ports with no job vacancies are more likely to have excess service capacity. The latter ports can thus take on the additional business from the former.

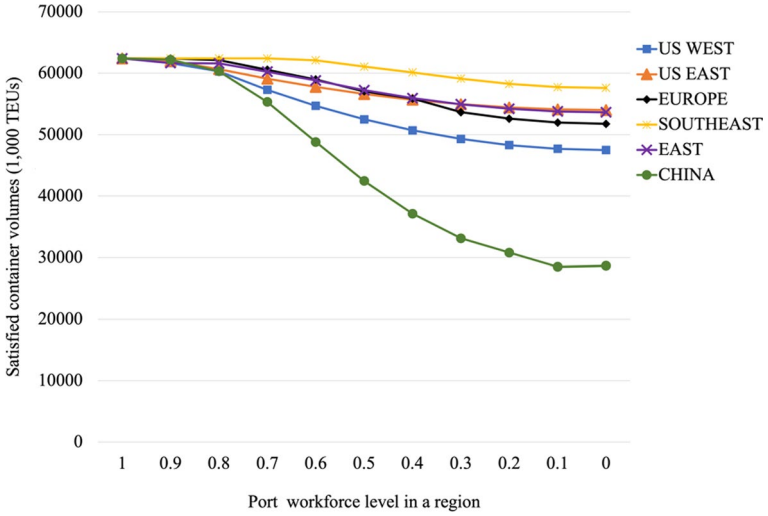

Fig. 4 Satisfied demand by changing the workforce level in any one of six regions

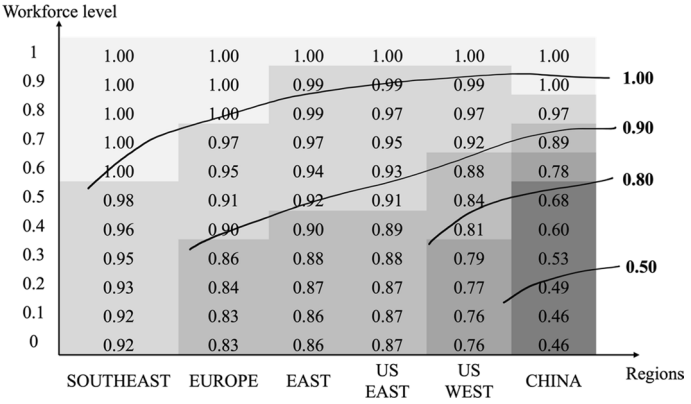

Fig. 5 Curves of satisfied demand rates by changing workforce levels in a region

Table 1 lists network-wide port throughputs for the regional runs. Network-wide port throughput from Run 0 is 178,563,997 TEUs. With regional workforce levels at the ports decreasing from 1 (100% of positions are filled), network-wide port throughput increases (in bold) and then decreases. The maximum increase in network-wide port throughput is 5%, arising under a workforce level of 0.9 in the US EAST. This increase is due to added transshipments required to avoid a region with a worker shortage and meet delivery requirements. The maximum decrease in network-wide port throughput at 54% arises in the case of full closure of the ports in CHINA. A result of the closures is that no imports, exports, or transshipment of containers can occur at these ports. With China's significant market share, particularly in exports, the impact on total container flows in the network is very large.

Table 1 Network-wide port throughput by changing workforce levels in a region

Workforce level	SOUTHEAST	EUROPE	EAST	US EAST	US WEST	CHINA
1	178,563,997	178,563,997	178,563,997	178,563,997	178,563,997	178,563,997
0.9	**178,807,978**	**179,367,986**	**185,384,011**	**187,775,995**	**186,718,473**	**185,383,436**
0.8	**179,104,489**	**184,541,803**	**179,770,646**	**184,136,027**	**183,472,134**	172,586,859
0.7	**180,817,274**	**181,187,987**	171,688,029	177,755,991	165,756,013	156,310,009
0.6	**184,930,401**	174,986,982	164,858,725	169,463,933	159,456,011	130,864,058
0.5	**180,196,912**	169,776,018	162,327,961	167,807,821	153,671,429	112,512,036
0.4	175,936,906	166,376,017	161,300,001	167,779,987	152,439,994	101,504,024
0.3	172,591,999	162,747,957	153,707,945	167,423,972	145,728,005	90,640,025
0.2	167,186,631	157,861,317	153,008,001	166,586,620	143,132,000	89,200,009
0.1	166,536,002	155,160,000	146,432,001	164,992,002	140,759,998	83,776,002
0	163,871,966	153,719,975	144,736,000	161,375,998	138,727,998	81,824,003

Consider also the Port of Singapore in the SOUTHEAST, under a workforce level of 0.6 (or with 40% of job vacancy). The majority of containers that arrive to and depart from the port, neither begin nor end their journeys there; that is, they are transshipments. Consequently, another port could readily serve these containers. The results show that, in fact, containers will divert to vessels served at other ports, under a worker shortage of this magnitude. Some containers will incur two or more transshipment operations as a result. This explains the observed increase in network-wide port throughput at 4% for the reduce workforce level in the SOUTHEAST.

In Table 1, the geographical areas with network-wide port throughputs greater than (in bold) the base of 178,563,997 TEUs per year aligns with the 1.00 curve plotted in Fig. 5. Although impacts of smaller scale regional port-related worker shortage scenarios – in terms of meeting O-D container demand – can be absorbed by the network, network-wide port throughput increases, increasing total transportation costs for the system.

5.2.2 Impacts on Other Regions

A correlation heatmap is provided in Fig. 6. The closer the correlation coefficient is to 1 or -1, the greater the impact of a shortage in one region on the other. For regions that are positively (negatively) correlated, a shortage in one region will lead to reduced (increased) total throughput in the ports of the other. The first row of the heatmap shows that a worker shortage in the CHINA region has the greatest impact on the US WEST region and the least impact on the SOUTHEAST region in terms of regional port throughput. The fifth row shows that the EUROPE, US EAST, and SOUTHEAST regions can benefit from a worker shortage in the EAST region.

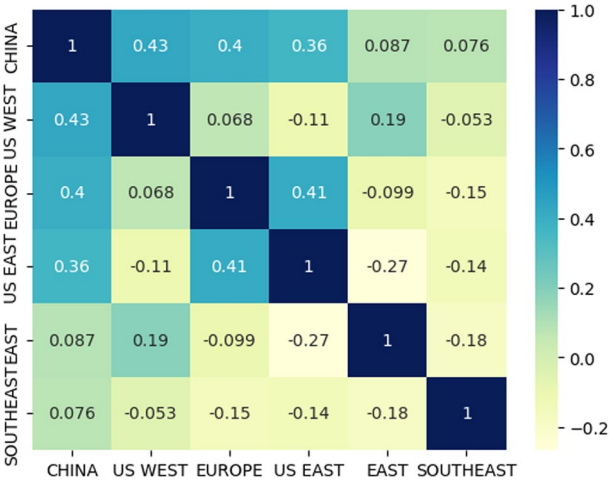

Fig. 6 Correlation heatmap

6 Conclusions and Discussion

This paper proposes a Maritime Cargo Flow Optimization Model, a MILP, for determining an optimal set of containerized vessel flows under given labor levels. An exact methodology that exploits Benders decomposition and column generation is used for its solution. The model and algorithm were employed on a port network representation including 77 ports, 32 routes, 338 links, and 4,110 legs to assess the impacts of port-related worker shortages on network-wide and regional port performance using a variety of metrics.

Findings from these numerical experiments indicate that low- and even medium-level, network-wide worker shortages can be absorbed, but with changes in port usage and increased transshipments, i.e., at a greater cost to shippers. Further, when a worker shortage arises in some key regions, e.g., CHINA, the impacts for key partner regions can be significant. For example, a closure of ports in CHINA would lead to a 54% reduction in network-wide port throughput. Of the 54-percentage reduction, 15 percentage points come directly from inbound and outbound demand that cannot be served. With a 70% reduction in labor at the same ports in China, the network-wide reduction in total port throughput would remain at 47%. In fact, through rerouting, other regions gain in these circumstances. Furthermore, curves of satisfied demand rates show that at an across-the-board shortage of more than 40%, the maritime system will not be able to absorb the impacts. An across-the-board shortage could reflect a situation with unfulfilled job vacancies due to a lack of skilled dockworkers. Since below this level, the impact can be absorbed, albeit at a cost, it appears that there may exist a critical level of job vacancies or extended absenteeism.

Finally, understanding the interregional interactions can inform the development of alliances between ports and/or regions aimed at reducing their exposure to the impacts

of worker shortages. For example, ports can develop strategic partnerships or coalitions for times of significant disruption as in a climate-related event. During such an event, coalition members would provide capacity to other member ports, enabling the affected port to serve a significant part of its customers along alternative routes (Li et al. 2022). Such coalitions produce greater service reliability for their members. These findings can inform port authorities who cooperate with unions, representing dockworkers and industry groups that represent maritime shippers, to better prepare for worker shortages. The findings also suggest the importance of maintaining a pipeline of skilled workers and, perhaps, can inform port authorities on the value of retaining workers when unfulfilled job vacancies begin to grow.

Additional experiments would be required to analyze the effects of shorter-term worker shortages or shortages that increase and decrease over time. A deeper understanding of the effects of worker shortage dynamics can support operational decisions during times when positions are difficult to fill or worker absenteeism varies and differs from expected levels. The effects of even short-term events can have important impact. For example, the Ports of Los Angeles and Long Beach were closed for approximately 24 h on April 7 of 2023, due to walkout. This instance of worker absence led to significant delays that cascaded through the maritime system, diminishing confidence by ocean carriers in the U.S. West Coast to deliver needed port services (Gerber and White 2023). To capture the effects of variability in worker level over time, a transient analysis would be required. The proposed model and solution method can be extended to support such an analysis.

Historical operational data from real-world port worker shortage scenarios, such as those during the early period of the COVID-19 pandemic, can be analyzed to best characterize the workforce level-dependent performance function. With a deeper understanding of this function, worker shortage impacts can be more accurately quantified through numerical experimentation as provided herein. The proposed model can handle any relationship. For a nonlinear, nonconvex relationship, linear approximation may be required.

The methodology developed here (Appendix A) can readily support investigation of the impacts of unfulfilled job vacancies and absenteeism in other aspects of cargo logistics systems, including vessel crews and customs workers. These applications will also require development of workforce level-dependent performance functions appropriate to their settings. The network representation can be expanded to include ground transportation and storage capacity, to capture even more details of the logistics system. Additional experiments on such an expanded network representation could elucidate the affects of workforce level reductions or absenteeism in these other aspects of the logistic system. Other forms of disruption, such as threat of attack at a border crossing, train derailment or facility capacity reduction, or closures from other portions of the logistics system, can also be assessed with the proposed methodology.

Appendix A: Mathematical Formulation and Solution Methodology

This appendix presents the mathematical formulation of the cargo flow optimization model and provides details of an exact methodology for its solution. Notation used in the formulation is presented in Table 2.

Table 2 Notation

Sets	
P	Ports
Φ	Routes
K	Links
L	Legs defined in terms of constituent links
$L(\phi)$	Legs used in route ϕ
$K(\phi)$	Links used in route ϕ
$K\left(l_{\phi}^{v}(i,j)\right)$	Links used in leg $l_{\phi}^{v}(i,j)$ starting at port i and ending at port j operated by vessel of type v on route ϕ
OD	Origin–destination (O-D) pairs
V	Vessel types
S_{od}	Paths that are available for shipments with od pair od ∈ OD
$S\left(l_{\phi}^{v}(i,j)\right)$	Paths that use leg $l_{\phi}^{v}(i,j)$ starting at port i and ending at port j operated by vessel of type v on route ϕ
Parameters	
r_p	Workforce level for port $p, p \in P$
$t(r_p)$	Cargohandling time at port p, $p \in P$ given operating rate r_p
h_p	Cargohandling time at port $p, p \in P$ when fully staffed
$\text{cap}(r_p)$	Service capacity in 1,000 TEUs at port p given workforce level $r_p, p \in P$
cap_p	Service capacity in 1,000 TEUs at port $p, p \in P$ when fully staffed
c_p	Fixed handling cost per 1,000 TEUs at port p, $p \in P$
$l_{\phi}^{v}(i,j)$	Leg starting from port i and ending at port j, operated by vessels of type v on route ϕ
$t\left(l_{\phi}^{v}(i,j)\right)$	Shipping time associated with leg $l_{\phi}^{v}(i,j)$ starting at port i and ending at port j operated by vessel of type v on route ϕ
$c\left(l_{\phi}^{v}(i,j)\right)$	Cargohandling costs along leg $l_{\phi}^{v}(i,j)$ charged for loading at port i and unloading at port j when operated by vessels of type v on route ϕ
$k_{\phi}^{v}(i,j)$	Link starting from port i and ending at port j operated by vessel of type v on route ϕ
$t\left(k_{\phi}^{v}(i,j)\right)$	Shipping time associated with link $k_{\phi}^{v}(i,j)$ starting at port i and ending at port j operated by vessel of type v on route ϕ, where speed depends on the vessel type
c_{ϕ}^{v}	Operational costs, including such voyage costs as bunker fuel, insurance premiums, and tariffs by canal, for route ϕ when operated by vessel of type v
s_{od}	Path from origin port o to destination port d, od ∈ OD
$c_s(\text{od})$	Cost of shipping cargo from an origin port o to a destination port d along path s_{od}
$t_s(\text{od})$	Shipping time for path s_{od}, od ∈ OD
$L\left(s_{\text{od}}\right)$	Legs used in path s_{od}, od ∈ OD
$f_s\left(t_s(\text{od})\right)$	Delay penalties in $ for path s_{od}, od ∈ OD
D_{od}	Cargo shipment demand for od ∈ OD
$\zeta_{kl\phi}$	= 1, indicating link k ($k_{\phi}^{v}(i,j)$) is used by leg l ($l_{\phi}^{v}(i,j)$)along route ϕ; = 0, otherwise
cap_v	Carrying capacity for vessel of type v
cap_{ϕ}^{v}	Available number of transits (in trips by vessels per year) for vessels of type v along route ϕ
ω	Penalties in $ for unsatisfied demand

Table 2 (continued)

Sets	
P	Ports
Decision variables	
f_{ϕ}^{v}	Number of vessel transits for vessels of type v assigned to each route ϕ
$z_s(\text{od})$	Containerized cargo in 1,000 TEUs shipped along each path s_{od}, od ∈ OD
$y_{\phi}^{v}(i,j)$	Containerized cargo in 1,000 TEUs shipped along each leg $l_{\phi}^{v}(i,j)$ starting at port i and ending at port j operated by vessel of type v on route ϕ
u_{od}	Unsatisfied demand for each od ∈ OD

$$\text{Problem } P(r_p) \text{ (given, } r_p, \ \forall p \in P)$$

$$\text{Minimize} \sum_{v \in V} \sum_{\phi \in \Phi} c_{\phi}^{v} \cdot f_{\phi}^{v} + \sum_{\text{od} \in \text{OD}} \sum_{s_{\text{od}} \in S_{\text{od}}} \left(c_{\text{s}}(\text{od}) \cdot z_{\text{s}}(\text{od}) \right) + \omega \cdot \sum_{\text{od} \in \text{OD}} u_{\text{od}} \tag{7}$$

subject to

$$\sum_{s_{\text{od}} \in S_{\text{od}}} z_{\text{s}}(\text{od}) = D_{\text{od}} - u_{\text{od}}, \forall \text{od} \in \text{OD} \tag{8}$$

$$\sum_{\text{od} \in \text{OD}} \sum_{s_{\text{od}} \in S\left(l_{\phi}^{v}(i,j)\right)} z_{\text{s}}(\text{od}) \leq y_{\phi}^{v}(i,j), \forall v \in V, \phi \in \Phi, l_{\phi}^{v}(i,j) \in L(\phi) \tag{9}$$

$$\sum_{l_{\phi}^{v}(i',j') \in L(\phi)} \zeta_{kl\phi} \cdot y_{\phi}^{v}\left(i',j'\right) \leq \text{cap}_{v} \cdot f_{\phi}^{v}, \forall v \in V, \phi \in \Phi, k_{\phi}^{v}(i,j) \in K(\phi) \tag{10}$$

$$f_{\phi}^{v} \leq \text{cap}_{\phi}^{v}, \forall v \in V, \phi \in \Phi \tag{11}$$

$$\sum_{v \in V} \sum_{\phi \in \Phi} \sum_{l_{\phi}^{v}(i,p), l_{\phi}^{v}(p,j) \in L(\Phi)} \left(y_{\phi}^{v}(i,p) + y_{\phi}^{v}(p,j) \right) \leq \text{cap}\left(r_p\right), \forall p \in P \tag{12}$$

$$f_{\phi}^{v} \in \mathbb{Z}_{+} \ \forall v \in V, \phi \in \Phi \tag{13}$$

$$z_s(od), y_{\phi}^{v}(i,j), u_{\text{od}} \in \mathbb{R}_{+}, \ \forall s_{\text{od}} \in S_{\text{od}}, v \in V, \phi \in \Phi, l_{\phi}^{v}(i,j) \in L(\phi), \ \text{od} \in \text{OD} \tag{14}$$

Objective function (7) is a generalized cost function consisting of three terms: (i) total route operational costs, (ii) total transportation costs, and (iii) penalties for unsatisfied demand. Total route operational costs depend on the decisions of the number of vessel transits for vessels of type v assigned to each route ϕ, f_{ϕ}^{v},

and operational costs of route ϕ when operated by vessel of type v, c^v_ϕ. Total transportation costs are obtained from path-based costs,c_s(od), over all paths, s_{od} ,od ∈ OD, through Eq. (15). Transportation costs include cargohandling costs charged at ports for loading and unloading tasks, costs for transport along constituent legs $c\left(l^v_\phi(i,j)\right)$, and delay penalties $f_s\left(t_s(\text{od})\right)$, where $f_s\left(t_s(\text{od})\right)$ is computed from path shipping time t_s(od) as in Eq. (16). Path-based transit times are computed from leg transit times, $t\left(l^v_\phi(i,j)\right)$, obtained via Eq. (17) and given workforce level-dependent cargohandling times $t\left(r_p\right)$. Finally, penalty ω is applied per unit of unsatisfied demand u_{od} over all od ∈ OD.

$$c_s(od) = \sum_{l^v_\phi(i,j)\in L\left(s_{od}\right)} c\left(l^v_\phi(i,j)\right) + f_s\left(t_s(od)\right), \forall od \in OD, s_{od} \in S_{od} \tag{15}$$

$$t_s(od) = \sum_{l^v_\phi(i,j)\in L\left(s_{od}\right)} t\left(l^v_\phi(i,j)\right), \forall od \in OD, s_{od} \in S_{od} \tag{16}$$

$$t\left(l^v_\phi(i,j)\right) = \sum_{k^v_\phi(i,j)\in K\left(l^v_\phi(i,j)\right)} t\left(k^v_\phi(i,j)\right) + t\left(r_i\right) + t\left(r_j\right), \forall v \in V, \phi \in \Phi, l^v_\phi(i,j) \in L(\phi) \tag{17}$$

Constraints (8) compute met demand by OD pair. This path-based demand is served by legs as defined by constraints (9). Constraints (10) ensure that the total flow along any link will not exceed the link's capacity. Total flow along any link is the sum of flows along legs that use the link. Link capacities are a function of number of transits made along routes served by this link. Vessel transit limits are guided by constraints (11). Together, constraints (8) through (11) ensure flow conservation and capacity limitations are met. Workforce level-dependent port throughput capacities, $\text{cap}\left(r_p\right)$, constrain inbound and outbound cargo flows at each port p in constraints (12). Integrality of f^v_ϕ and nonnegativity in z_s(od), $y^v_\phi(i,j)$, and u_{od} are ensured through constraints (13) and (14), respectively. Model P(r_p) is, thus, a mixed-integer, linear program (MILP).

The Bureau of Transportation Statistics (2017) states that port throughput capacity depends not only on the physical constraints of the port, but also on its operations. Thus, port throughput capacity depends on hours of operation, workforce level, and operating methods at each terminal. Workforce level r_p for port p, taken between 0 and 1, is computed as the ratio of the available to required number of port workers, where the required number implies that the port can reach its full throughput capacity. The presence of more than the necessary number of workers will have no added benefit.

Equations (18, 18′ and 18″) connect the workforce level-dependent cargohandling times and capacities at the ports under three presumed relationships, linear, square and exponential, respectively. These are referred to as workforce level-dependent performance functions. An exponential relationship of cargohandling times with delays at ports is assumed in (Schofer et al. 2022). Parameters h_p and cap_p represent the cargohandling time and service capacity, respectively, at port p given full worker

availability. h_p is set as 2 or 3 days depending on port size, with less time required at larger ports. To eliminate the possibility of division by zero, if r_p is 0, a very small number is used in its place, creating excessively large cargohandling times and near-zero capacities.

$$\text{Linear} \quad t(r_p) = h_p \cdot \left(\frac{1}{r_p}\right), \ \forall p \in P \tag{18}$$

$$\begin{aligned} &\text{Square} \quad t(r_p) = h_p \cdot \left(\frac{1}{r_p}\right)^2, \ \forall p \in P \\ &\text{cap}(r_p) = \text{cap}_p \cdot (r_p)^2, \ \forall p \in P \end{aligned} \tag{18′}$$

$$\begin{aligned} &\text{Exponential} \quad t(r_p) = (h_p)^{\frac{1}{r_p}}, \ \forall p \in P \\ &\text{cap}(r_p) = \text{cap}_p^{r_p}, \ \forall p \in P \end{aligned} \tag{18″}$$

The notation and link-leg-based network representation used herein follow closely with maritime flow models presented in earlier works, including Asadabadi and Miller-Hooks 2002; Achurra-Gonzalez et al. 2019; and Li et al. 2022. The optimization model is adapted from the Risk-constrained Maritime Cargo Flow Optimization Model proposed in Li and Miller-Hooks (in review). This adapted model excludes risk-based factors and constraints associated with passage through the Arctic Sea, the subject of their work, but adds constraints and extra costs to capture the effects of worker levels on operational efficiency.

Solution Methodology with Benders Decomposition and Column Generation

Solution of P(r_p) is nontrivial as the number of path-based decision variables z_s(od) increases exponentially with problem size. For large instances as considered herein, the model can be solved by Benders decomposition (Benders, 1962) and column generation. Specifically, P(r_p) is decomposed into a Benders master problem, MP(r_p), with integer decision variables and a Benders subproblem, SP(r_p), with path-based continuous decision variables. The path-based subproblem can be solved through column generation, potentially significantly reducing the number of paths that must be considered. Given the limited path set and integer solutions, $\overline{f_\phi^v}$, from MP(r_p), the resulting Benders SP(r_p) is a pure linear program. Dual variables $\left(\delta_{\text{od}}, \kappa\left(l_\phi^v(i,j)\right), \varphi_p, \pi\left(k_\phi^v(i,j)\right), \forall \text{od} \in \text{OD}, s_{\text{od}} \in S_{\text{od}}, v \in V, \phi \in \Phi, k_\phi^v(i,j) \in K(\phi), l_\phi^v(i,j) \in L(\phi)\right)$ are associated with constraints (8), (9), (12), and (20), respectively. Given these dual variables, the dual of SP(r_p) is formulated as DSP(r_p). MP(r_p), SP(r_p), and DSP(r_p) are given next. An overview of the solution framework is given in Fig. 7.

1 Initialization
1.1 Initialize upper bound $z_u = +\infty$ and lower bound $z_l = -\infty$.
1.2 Set the gap tolerance as ϵ .

2 Tolerance satisfaction $z_u - z_l > \epsilon$
2.1 Solve Benders MP(r_p) to obtain optimal solutions ($\bar{f}_\phi^v$, $\bar{\tau}$).
2.2 Solve Benders SP(r_p) given $\bar{f}_\phi^v$ and limited path sets, and generate Benders cuts.
2.3 Append Benders cuts into Benders MP(r_p).
2.4 Update lower bounds
$$z_l = \max\{z_l, \sum_{v\in V}\sum_{\phi\in\Phi} c_\phi^v \cdot f_\phi^v + \tau\}.$$
2.5 Update upper bounds
$$z_u = \min\{z_u, \sum_{v\in V}\sum_{\phi\in\Phi} c_\phi^v \cdot \bar{f}_\phi^v + \sum_{od\in OD}\sum_{s\in S_{od}}(c_s(od) \cdot z_s(od)) + \omega \cdot \sum_{od\in OD} u_{od}\}.$$

3 Termination
Stop.

Fig. 7 Overview of Benders decomposition solution procedure

Problem SP(r_p) (given $r_p, \forall p \in P$)

$$\text{Minimize} \sum_{od\in OD}\sum_{s_{od}\in S_{od}} \left(c_s(od) \cdot z_s(od)\right) + \omega \cdot \sum_{od\in OD} u_{od} \tag{19}$$

subject to
(8), (9), (12), (14)

$$\sum_{l_\phi^v(i,j)\in L(\phi)} \zeta_{kl\phi} \cdot y_\phi^v(i,p) \le cap_v \cdot \bar{f}_\phi^v, \forall v \in V, \phi \in \Phi, k_\phi^v(i,j) \in K(\phi) \tag{20}$$

Problem DSP(r_p) (given $r_p, \forall p \in P$)

$$\text{Maximize} \sum_{od\in OD} D_{od} \cdot \delta_{od} + \sum_{v\in V}\sum_{\phi\in\Phi}\sum_{k_\phi^v(i,j)\in K(\phi)} \left(cap_v \cdot f_\phi^v \cdot \pi\left(k_\phi^v(i,j)\right)\right) + \sum_{p\in P} cap(r_p) \cdot \varphi_p \tag{21}$$

subject to

$$\delta_{od} + \sum_{l_\phi^v(i,j)\in K(\phi)} \kappa\left(l_\phi^v(i,j)\right) \le c_s(od), \forall od \in OD, s_{od} \in S_{od} \tag{22}$$

$$-\kappa\left(l_\phi^v(i,j)\right) + \sum_{k_\phi^v(i,j)\in K(\phi)} \pi\left(k_\phi^v(i,j)\right) + \varphi_i + \varphi_j \le 0, \forall v \in V, \phi \in \Phi, l_\phi^v(i,j) \in L(\phi) \tag{23}$$

$$\begin{aligned}&\delta_{od} \text{ unrestricted, } \kappa\left(l_{\phi}^{v}(i,j)\right), \pi\left(k_{\phi}^{v}(i,j)\right), \varphi_{p} \in \mathbb{R}^{-},\\ &\forall od \in OD, s_{od} \in S_{od}, v \in V, \phi \in \Phi, k_{\phi}^{v}(i,j) \in K(\phi), l_{\phi}^{v}(i,j) \in L(\phi)\end{aligned} \tag{24}$$

$$\text{Problem MP}(r_p)\ (given,\ r_p,\ \forall p \in P)$$

$$\text{Minimize} \sum_{v \in V} \sum_{\phi \in \Phi} c_{\phi}^{v} \cdot f_{\phi}^{v} + \tau \tag{25}$$

subject to

(11), (13)

$$\tau \geq \sum_{od \in OD} D_{od} \cdot \delta_{od} + \sum_{v \in V} \sum_{\phi \in \Phi} \sum_{k_{\phi}^{v}(i,j) \in K(\phi)} \left(cap_{v} \cdot f_{\phi}^{v} \cdot \pi\left(k_{\phi}^{v}(i,j)\right)\right) + \sum_{p \in P} cap\left(r_p\right) \cdot \varphi_{p} \tag{26}$$

Solution of the Benders MP(r_p) produces integer decisions $\overline{f_{\phi}^{v}}$ and continuous decision $\overline{\tau}$. Its optimal objective value is used as an upper bound on program P(r_p). These integer decisions, $\overline{f_{\phi}^{v}}$, provide input to the Benders SP(r_p). Dual solutions of the Benders SP(r_p) are used to generate Benders cuts and provide lower bounds on program P(r_p). As any solutions from the Benders MP(r_p) are feasible to the Benders SP(r_p), only optimality cuts are generated. These Benders cuts (constraints (26)) are used to constrain the Benders MP(r_p) in the next iteration. Note that the initial MP(r_p) is a relaxed version of the original problem P(r_p) as it has only integer decision variables, f_{ϕ}^{v}, and constraints (11) and (13) associated with the integer variables. The algorithm iterates by solving the Benders MP constrained by added Benders cuts to produce integer solutions, $\overline{f_{\phi}^{v}}$, and updated upper bounds. The algorithm terminates when the gap between the upper and lower bounds is less than a predefined tolerance ϵ.

In solving Benders SP(r_p), a master problem and a subproblem are generated through decomposition of Benders SP(r_p). The subproblem is a shortest path problem. Given a path $s_{\text{od}} \in S_{\text{od}}$ and dual variables δ_{od} and $\kappa(l_{\phi}^{v}(i,j))$, the reduced cost of path s_{od}, $\overline{c_s(\text{od})}$, can be computed by Eq. (27). Note that only the first and last terms are leg-based and, thus, path-based computations are required. The label correcting method with added fathoming rules is used to solve the subproblem and find negative-valued, reduced-cost paths. These paths are added to an expanding path set. This path set is used to solve the master problem. The column generation procedure terminates when no new paths with negative reduced costs can be found.

$$\overline{c_s(od)} = \sum_{l_{\phi}^{v}(i,j) \in L\left(s_{od}\right)} c\left(l_{\phi}^{v}(i,j)\right) + f_s\left(\sum_{l_{\phi}^{v}(i,j) \in L\left(s_{od}\right)} t\left(l_{\phi}^{v}(i,j)\right)\right) - \delta_{od} - \sum_{l_{\phi}^{v}(i,j) \in L\left(s_{od}\right)} \kappa\left(l_{\phi}^{v}(i,j)\right) \tag{27}$$

Appendix B: Containerized Cargo Demand

ID	Origin	Destination	Volume (1000 TEUs)
0	Ningbo	Antwerp	560
1	Busan	Rotterdam	800
2	Antwerp	New York	400
3	Shenzhen	Hamburg	840
4	Shanghai	Rotterdam	1120
5	Shanghai	New York	2000
6	Ningbo	New York	2000
7	Guangzhou	Hamburg	560
8	Rotterdam	Norfolk	1200
9	Shenzhen	Rotterdam	560
10	Antwerp	Xiamen	280
11	Hamburg	Busan	280
12	Ningbo	Miami	1200
13	Shenzhen	Algeciras	280
14	Algeciras	Qingdao	560
15	Yokohama	Charleston	800
16	Ningbo	Algeciras	280
17	Antwerp	Charleston	400
18	Xiamen	Baltimore	400
19	Ningbo	Bremerhaven	280
20	Bremerhaven	Houston	800
21	Bremerhaven	Hong Kong	520
22	Shanghai	Bremerhaven	420
23	Qingdao	Beirut	280
24	Hong Kong	Houston	2000
25	Xiamen	Savannah	2000
26	Felixstowe	Savannah	800
27	Guangzhou	Antwerp	840
28	Tianjin	Los Angeles	1120
29	Shanghai	Long Beach	2400
30	Xiamen	Oakland	1200
31	Long Beach	Ningbo	400
32	Qingdao	Los Angeles	1400
33	Singapore	Long Beach	1200
34	Singapore	Los Angeles	800
35	Los Angeles	Hong Kong	800
36	Oakland	Tokyo	800
37	Shenzhen	Oakland	800
38	Xiamen	Felixstowe	840
39	Zeebrugge	Kaohsiung	420

ID	Origin	Destination	Volume (1000 TEUs)
40	Shenzhen	Southampton	420
41	Guangzhou	Vancouver	1040
42	Qingdao	Seattle	1600
43	Yokohama	Seattle	1200
44	Shenzhen	Alexandria	392
45	Qingdao	Ashdod	392
46	Qingdao	Barcelona	840
47	Shanghai	Vancouver	2000
48	Ningbo	Valencia	1200
49	Venice	Busan	140
50	Gdansk	Taipei	400
51	Tianjin	Trieste	240
52	Tianjin	Piraeus	1200
53	Dubai	Tokyo	840
54	Tianjin	La Spezia	400
55	Genoa	Osaka	560
56	Busan	Odessa	196
57	Port Said	Qingdao	700
58	Fos	Busan	280
59	Fuzhou	Colon	1200
60	Colon	Busan	320
61	Colombo	Shanghai	1600
62	Dalian	Dubai	720
63	Constantza	Koper	200
64	Busan	Le Havre	560
65	Tianjin	Malta	400
66	Tianjin	Mersin	600
67	Qingdao	Prince Rupert	224
68	Haifa	Qingdao	336
69	Istanbul Ambarli	Busan	840
70	Kaohsiung	Jeddah	1600
71	Mobile	Dunkirk	120
72	Busan	New Orleans	600
73	Guangzhou	Dubai	1400
74	Guangzhou	Halifax	140
75	Jakarta	Guangzhou	560
76	Shenzhen	Jakarta	560
77	Shanghai	Jakarta	560
78	Hong Kong	Oakland	1200

Table 3 Port and port-related parameters

ID	Port,$p \in P$	Throughput capacity (1,000 TEUs) $\text{cap}_p, \forall p \in P$	Handling Time (days) $h_p, \forall p \in P$	Port handling cost (1,000$/1,000 TEUs) $c_p, \forall p \in P$
0	Alexandria	800	3	300
1	Algeciras	2000	2	200
2	Altamira	800	3	300
3	Antwerp	8000	2	200
4	Ashdod	800	3	300
5	Baltimore	600	3	300
6	Barcelona	2000	2	200
7	Beirut	600	3	300
8	Boston	200	3	300
9	Bremerhaven	3200	2	200
10	Busan	10,000	2	200
11	Cai Mep	3200	2	200
12	Charleston	1200	3	300
13	Colombo	3200	2	200
14	Colon	2000	2	200
15	Constanța	600	3	300
16	Dalian	1200	2	200
17	Dubai	6000	2	200
18	Dunkirk	200	3	300
19	Felixstowe	3200	2	200
20	Fos	600	3	300
21	Fuzhou	1600	2	200
22	Gdansk	800	3	300
23	Genoa	1200	3	300
24	Guangzhou	10,000	2	200
25	Haifa	600	3	300
26	Halifax	200	3	300
27	Hamburg	4000	2	200
28	Hong Kong	8000	2	200
29	Houston	3200	3	300
30	Istanbul Ambarli	1600	3	300
31	Jakarta	3600	2	200
32	Jeddah	2000	2	200
33	Kaohsiung	4800	2	200
34	Koper	400	3	300
35	La Spezia	800	3	300
36	Laem Chabang	3400	2	200
37	Le Havre	1200	3	300
38	Long Beach	6000	2	200
39	Los Angeles	6000	2	200
40	Malta	1400	3	300

Table 3 (continued)

ID	Port,$p \in P$	Throughput capacity (1,000 TEUs) $\text{cap}_p, \forall p \in P$	Handling Time (days) $h_p, \forall p \in P$	Port handling cost (1,000$/1,000 TEUs) $c_p, \forall p \in P$
41	Mersin	800	3	300
42	Miami	1200	3	300
43	Mobile	200	3	300
44	New Orleans	800	3	300
45	New York	6000	2	200
46	Ningbo	11,200	2	200
47	Norfolk	2000	3	300
48	Oakland	4000	3	300
49	Odessa	200	3	300
50	Osaka	1000	3	300
51	Piraeus	2000	2	200
52	Port Kelang	4000	2	200
53	Port Said	1400	3	300
54	Prince Rupert	520	3	300
55	Qingdao	8000	2	200
56	Rijeka	100	3	300
57	Rotterdam	6000	2	200
58	Savannah	3200	2	200
59	Seattle	4000	2	200
60	Shanghai	16,000	2	200
61	Shenzhen	12,000	2	200
62	Singapore	15,200	2	200
63	Southampton	800	3	300
64	Taipei	800	3	300
65	Tampa	200	3	300
66	Tanjung Pelepas	3600	2	200
67	Tianjin	6000	2	200
68	Tokyo	2000	2	200
69	Trieste	400	3	300
70	Valencia	2000	2	200
71	Vancouver	4000	2	200
72	Venice	400	3	300
73	Veracruz	400	3	300
74	Xiamen	6000	2	200
75	Yokohama	2400	3	300
76	Zeebrugge	800	3	300

Appendix C: Ports

The maritime system data used in this study were obtained from (Li et al. 2021), where a detailed global maritime network was developed using publicly available data sources, including details of the routes and related ports used by the 2 M Alliance. Relevant data are repeated here (Table 3).

Appendix D: Routes

Modeled routes incorporated in the creation of the network tested herein were developed from scheduled loops of the 2 M Alliance as described in (Li et al. 2021). The relevant routes to this study are given here for completeness.

ID	Route
0	Shanghai, Ningbo, Xiamen, Shenzhen, Singapore, Felixstowe, Zeebrugge, Gdansk, Bremerhaven, Piraeus, Port Kelang, Hong Kong, Shanghai
1	Tianjin, Dalian, Qingdao, Shanghai, Ningbo, Singapore, Piraeus, Rotterdam, Hamburg, Antwerp, Rotterdam, Shanghai, Tianjin
2	Xiamen, Guangzhou, Hong Kong, Shenzhen, Cai Mep, Port Kelang, Piraeus, Hamburg, Rotterdam, Zeebrugge, Felixstowe, Singapore, Shenzhen, Xiamen
3	Busan, Ningbo, Shanghai, Shenzhen, Singapore, Algeciras, Southampton, Dunkirk, Hamburg, Rotterdam, Southampton, Le Havre, Malta, Dubai, Port Kelang, Xiamen, Busan
4	Qingdao, Ningbo, Shanghai, Shenzhen, Cai Mep, Singapore, Le Havre, Rotterdam, Hamburg, Antwerp, Le Havre, Algeciras, Port Kelang, Guangzhou, Qingdao
5	Kaohsiung, Qingdao, Ningbo, Shanghai, Taipei, Shenzhen, Tanjung Pelepas, Rotterdam, Felixstowe, Hamburg, Rotterdam, Colombo, Tanjung Pelepas, Kaohsiung
6	Shanghai, Ningbo, Kaohsiung, Shenzhen, Colombo, Antwerp, Hamburg, Rotterdam, Port Kelang, Shanghai
7	Qingdao, Shanghai, Ningbo, Kaohsiung, Hong Kong, Shenzhen, Singapore, Piraeus, La Spezia, Genoa, Fos, Valencia, Piraeus, Colombo, Singapore, Hong Kong, Qingdao
8	Qingdao, Tianjin, Busan, Shanghai, Ningbo, Guangzhou, Shenzhen, Singapore, Malta, Valencia, Barcelona, Fos, Genoa, Malta, Beirut, Jeddah, Port Kelang, Xiamen, Qingdao
9	Busan, Shanghai, Ningbo, Xiamen, Shenzhen, Singapore, Port Said, Beirut, Piraeus, Mersin, Istanbul Ambarli, Constantza, Odessa, Istanbul Ambarli, Mersin, Port Said, Jeddah, Port Kelang, Busan
10	Qingdao, Shanghai, Ningbo, Taipei, Shenzhen, Tanjung Pelepas, Port Kelang, Ashdod, Haifa, Alexandria, Mersin, Piraeus, Jeddah, Tanjung Pelepas, Shenzhen, Kaohsiung, Qingdao
11	Shanghai, Ningbo, Busan, Shenzhen, Singapore, Malta, Koper, Trieste, Rijeka, Venice, Koper, Malta, Port Said, Jeddah, Port Kelang, Shenzhen, Shanghai
12	Fuzhou, Guangzhou, Hong Kong, Shenzhen, Xiamen, Los Angeles, Oakland, Fuzhou
13	Tianjin, Qingdao, Shanghai, Ningbo, Prince Rupert, Long Beach, Oakland, Tianjin
14	Port Kelang, Singapore, Jakarta, Laem Chabang, Cai Mep, Los Angeles, Oakland, Hong Kong, Cai Mep, Singapore, Port Kelang, Colombo, Halifax, New York, Norfolk, Savannah, Charleston, Port Kelang
15	Qingdao, Shanghai, Ningbo, Los Angeles, Oakland, Tokyo, Qingdao

ID	Route
16	Kaohsiung, Cai Mep, Hong Kong, Shenzhen, Kaohsiung, Long Beach, Kaohsiung
17	Taipei, Xiamen, Shenzhen, Los Angeles, Oakland, Taipei
18	Shenzhen, Hong Kong, Kaohsiung, Taipei, Los Angeles, Oakland, Seattle, Kaohsiung, Shenzhen
19	Ningbo, Shanghai, Busan, Long Beach, Busan, Ningbo
20	Shenzhen, Xiamen, Ningbo, Shanghai, Busan, Seattle, Vancouver, Shenzhen
21	Hong Kong, Shenzhen, Ningbo, Shanghai, Prince Rupert, Vancouver, Yokohama, Shanghai, Hong Kong
22	Shenzhen, Kaohsiung, Shanghai, Ningbo, Seattle, Vancouver, Tokyo, Osaka, Qingdao, Shenzhen
23	Shenzhen, Hong Kong, Shenzhen, Kaohsiung, Vancouver, Seattle, Busan, Kaohsiung, Shenzhen
24	Qingdao, Ningbo, Shanghai, Busan, Colon, Savannah, Charleston, Boston, New York, Colon, Qingdao
25	Qingdao, Ningbo, Shanghai, Busan, New York, Norfolk, Savannah, Qingdao
26	Xiamen, Hong Kong, Shenzhen, Kaohsiung, Colon, Savannah, Baltimore, Norfolk, New York, Xiamen
27	Cai Mep, Hong Kong, Shenzhen, Xiamen, Shanghai, Colon, New York, Savannah, Charleston, Cai Mep
28	Shanghai, Ningbo, Xiamen, Shenzhen, Houston, Mobile, Tampa, Shanghai
29	Singapore, Hong Kong, Shenzhen, Ningbo, Shanghai, Busan, Houston, Mobile, New Orleans, Tampa, Miami, Singapore
30	Southampton, Antwerp, Rotterdam, Bremerhaven, Le Havre, New York, Norfolk, Savannah, Charleston, Southampton
31	Le Havre, Antwerp, Rotterdam, Bremerhaven, Charleston, Miami, Veracruz, Altamira, Houston, New Orleans, Le Havre

Acknowledgements This work was funded by U.S. National Science Foundation under Grant 1927785. This support is gratefully acknowledged but implies no endorsement of our findings. The authors are also grateful to the editor and reviewers for their helpful input that has helped to improve the paper.

Data availability The authors confirm that the data supporting the findings of this study are available within the article and its supplementary materials.

References

Achurra-Gonzalez, Pablo E., Matteo Novati, Roxane Foulser-Piggott, Daniel J. Graham, Gary Bowman, Michael GH. Bell, and Panagiotis Angeloudis. 2019. Modelling the impact of liner shipping network perturbations on container cargo routing: Southeast Asia to Europe application. *Accident Analysis & Prevention* 123: 399–410.

Asadabadi, Ali, and Elise Miller-Hooks. 2018. Co-opetition in enhancing global port network resiliency: a multi-leader, common-follower game theoretic approach. *Transportation Research Part b: Methodological* 108: 281–298.

Benders, Jacques F. 1962. Partitioning procedures for solving mixed-variables programming problems. *Numerische Mathematic* 4: 238–252.

Bureau of Transportation Statistics. 2017. Measures of throughput and capacity. https://www.bts.gov/archive/publications/port_performance_freight_statistics_annual_report/2016/ch3.

Cullinane, Kevin, and Hercules Haralambides. 2021. Global trends in maritime and port economics: the COVID-19 pandemic and beyond. *Maritime Economics & Logistics* 23: 369–380.

Ergun, Ozlem, Wallace J. Hopp, and Pinar Keskinocak. 2023. A structured overview of insights and opportunities for enhancing supply chain resilience. *IISE Transactions* 55 (1): 57–74.

Gerber, Marisa, and Ronald D. White. 2023. https://www.latimes.com/business/story/2023-04-07/la-ports-worker-shortage. Los Angeles Times.
Hu, Weihong, Mariel S. Lavieri, Alejandro Toriello, and Xiang Liu. 2016. Strategic health workforce planning. *IIE Transactions* 48 (12): 1127–1138.
Kay, Grace. 2021. Moody's warns of 'dark clouds ahead' for the global supply chain as 77% of the world's largest ports face backlogs. https://www.businessinsider.com/global-supply-chain-crisis-ports-face-record-delays-2021-10.
Kim, Sungjin, Soowon Chang, and Daniel Castro-Lacouture. 2020. Dynamic modeling for analyzing impacts of skilled labor shortage on construction project management. *Journal of Management in Engineering* 36 (1): 04019035.
Lewis, Brian M., Alan L. Erera, and Chelsea C. White III. 2006. Impact of temporary seaport closures on freight supply chain costs. *Transportation Research Record* 1963 (1): 64–70.
Li, Wenjie, Ali Asadabadi, and Elise Miller-Hooks. 2022. Enhancing resilience through port coalitions in maritime freight networks. *Transportation Research Part a: Policy and Practice* 157: 1–23.
Li, Wenjie, and Elise Miller-Hooks. in review. A risk-constrained maritime cargo flow optimization model for predicting changes in Arctic cargo vessel traffic under declining Arctic sea ice.
Li, Wenjie, Ralph Pundt, and Elise Miller-Hooks. 2021. An updatable and comprehensive global cargo maritime network and strategic seaborne cargo routing model for global containerized and bulk vessel flow estimation. *Maritime Transport Research* 2: 100038.
Merk, Olaf, Jan Hoffmann, and Hercules Haralambides. 2022. Post-COVID-19 scenarios for the governance of maritime transport and ports. *Maritime Economics & Logistics* 24: 673–685.
Miller-Hooks, Elise. 2023. Constructs in infrastructure resilience framing - from components to community services and the built and human infrastructures on which they rely. *IISE Transactions* 55 (1): 43–56.
Mongelluzzo, Bill. 2022a. LA-LB labor shortages dash hopes of CNY port recovery. https://www.joc.com/port-news/terminal-operators/la-lb-labor-shortages-dash-hopes-cny-port-recovery_2022a0202.html.
Mongelluzzo, Bill. 2022b. LA-LB terminals brace for COVID-related labor shortage. https://www.joc.com/port-news/us-ports/la-lb-terminals-brace-covid-related-labor-shortage_2022b0104.html.
Nagurney, Anna. 2021a. Supply chain game theory network modeling under labor constraints: applications to the Covid-19 pandemic. *European Journal of Operational Research* 293 (3): 880–891.
Nagurney, Anna. 2021b. Optimization of supply chain networks with inclusion of labor: applications to COVID-19 pandemic disruptions. *International Journal of Production Economics* 235: 108080.
Nagurney, Anna, and Alireza Ermagun. 2022. Resilience of supply chain networks to labor disruptions. Findings.
Notteboom, Theo, Thanos Pallis, and Jean-Paul. Rodrigue. 2021. Disruptions and resilience in global container shipping and ports: the COVID-19 pandemic versus the 2008–2009 financial crisis. *Maritime Economics & Logistics* 23: 179–210.
Notteboom, Theo, Athanasios Pallis, and Jean-Paul. Rodrigue. 2022. *Port economics, management and policy*. New York: Routledge.
Schofer, Joseph L., Hani S. Mahmassani, and Max TM. Ng. 2022. Resilience of US Rail intermodal freight during the COVID-19 pandemic. *Research in Transportation Business & Management* 43: 100791.
Shahverdi, Bahar, Mersedeh Tariverdi, and Elise Miller-Hooks. 2020. Assessing hospital system resilience to disaster events involving physical dam- age and demand surge. *Socio-Economic Planning Sciences* 70: 100729.
Statista. 2022. https://www.statista.com/statistics/1249648/leading-container-ship-alliances-market-share/

Wenjie Li has Ph.D. received her B.S., M.S., and Ph.D. degrees from Shandong Jianzhu University, Beijing Jiaotong University, and George Mason University, respectively. Her expertise and interests are in mathematical modeling and algorithms for maritime cargo flows, network optimization under uncertainty, and machine learning models for risk prediction. She will soon join BNSF Railway as Senior Specialist in Intermodal Analytics.

Elise Miller-Hooks Ph.D., holds the Hazel Endowed Chair in Infrastructure Engineering and is Interim Department Chair in Civil, Environmental and Infrastructure Engineering at George Mason University. She was a program director at the U.S. National Science Foundation and faculty at University of Maryland, Penn State and Duke University. She has received her Ph.D. in Civil Engineering from the University of Texas – Austin and B.S. in Civil Engineering from Lafayette College.